Turk J Elec Eng & Comp Sci, Vol.18, No.6, 2010, © TÜBİTAK
doi:10.3906/elk-0910-260

Delta-sigma subarray beamforming for ultrasound imaging

Hasan Şakir BİLGE
Department of Computer Engineering, Gazi University, Maltepe, 06570 Ankara-TURKEY
e-mail: bilge@gazi.edu.tr

Abstract

In this study, an ultrasonic digital beamformer based on subarray processing of 1-bit delta-sigma ($\Delta\Sigma$) oversampled echo signals is presented. The single-bit oversampling $\Delta\Sigma$ conversion simplifies the coherent processing in beamforming with improved timing accuracy. Subarray processing also aims to simplify the beamforming complexity, where the partial-beam sums (low-resolution beams) are acquired from small subarrays, and then these partial beams are coherently processed for producing high-resolution beams. In the $\Delta\Sigma$ subarray beamforming, the $\Delta\Sigma$ coded echo signals are summed over the subarray channels, and then these partial beam-sums are first $\Delta\Sigma$ demodulated, then processed for beam-interpolation, followed by coherent summation. This method requires decimation filtering of partial-beam sums from each subarray. The hardware complexity of the $\Delta\Sigma$ subarray beamformer is compared with other beamformers and significant front-end savings are explained. The system is tested experimentally and the results are compared with others using B-scan images reconstructed from archival experimental raw RF data. Both wire targets and cyst phantom are used to show the differences in Signal to Noise Ratio (SNR) and Contrast to Noise Ratio (CNR) measurements.

Key Words: *Delta-sigma conversion, beamforming, ultrasonic imaging*

1. Introduction

The array front-end and beamforming handle the data acquisition and coherent signal processing in ultrasound imaging, and thus critically affect the cost and performance of the overall imaging system. Advances in integrated circuit and transducer technologies push ultrasound array imaging systems to undergo significant developments. Current trends in ultrasound imaging are in the directions of full-scale real-time volumetric (3-D) imaging using 2-D arrays with thousands of elements, and miniature/micro devices such as portable imagers and intravascular/intracardiac imaging devices [1–8]. Design of low-cost and compact beamformers is crucial for realization of such systems, where reducing the cost, size, and power consumption of the front-end is critically important [9–17]. The phased array and synthetic aperture beamforming set the top and bottom boundaries

in array beamforming; the former produces the best beam quality but with the highest cost, whereas the latter offers the simplest beamformer but with poor beam quality. To simplify the array front-end and beamforming, researchers have investigated numerous approaches, such as multi-element synthetic aperture [18–21], sparse array [22–23], subarray [4, 24–26], and $\Delta\Sigma$ beamforming [27–38].

In this study, a new beamforming structure is considered which is based on both the subarray and $\Delta\Sigma$ beamforming approaches. These two approaches can be used together for miniaturization of the array front-end and/or funneling the electrical connections of large number of array elements into a reduced number of channels. The former approach reduces the number of active parallel channels by employing small subarrays in beam acquisition, whereas the latter approach simplifies the complexity of coherent processing by reducing the sample size to a single bit and increasing the timing accuracy through oversampling $\Delta\Sigma$ coding of the echo signals. In this method, decimation filtering is required for outputs of each subarray. The $\Delta\Sigma$ subarray beamforming is tested through digital emulations using archival experimental raw RF data. Some initial results are previously presented [33]. But in these figures, there are some fluctuations in B-mode images. This problem is solved by optimizing the filter parameters (beam interpolation and demodulation filters) in this paper. On the other hand, cyst phantom images, SNR and CNR measurements are added. The hardware complexities of different beamformers are compared. The proposed system is quantitatively investigated in detail in order to reveal its superiorities. Furthermore, a new alternative approach to combine subarray processing and $\Delta\Sigma$ beamforming is also proposed in discussion section. But a limited space is given to this new approach, because the SNR and CNR measurements, and final B-mode images are just the same with the detailed explained approach.

2. Digital beamforming methods

In this section, the digital beamforming methods are shortly reviewed. The state of the art in these techniques is summarized. These fundamental methods will be compared to the proposed one in the following sections, with the theoretical complexity parameters and experimental results.

2.1. Phased array beamforming

The widely used phased array beamformers are the gold-standard for ultrasonic beamforming, where all the transducers are actively used both in transmit and receive events. As a result of the parallel use of all array elements, it is necessary to use many front-end structures that include signal conditioning and analog-to-digital conversion circuitry, and also digital processing modules (hardware and/or software). The large aperture size of the phased array decreases the main-lobe width of the point spread function of the imaging system, and consequently increases the image resolution. The number of channels also determines directly the size, cost, and power need of the overall system.

In real-time imaging, the frame rate is inversely proportional to the number of firings per frame. This constraint can be given as:

$$f \leq \frac{c}{2R} \times \frac{1}{F}, \tag{1}$$

where f is the frame rate (frames/second), c is the velocity of ultrasound signal (m/s), R is the maximum imaging depth (m), and F is the number of firings per frame. In phased array configuration, F is also equal to

the maximum number of beam lines in a frame. If F=200 is taken as an usual case, which gives a quite good image quality, then f becomes approximately 24 for a 150 mm depth imaging with a sound velocity of 1480 m/s. This frame rate is fairly enough for good quality.

2.2. $\Delta\Sigma$ beamforming

In digital beamforming using oversampled 1-bit $\Delta\Sigma$ coded data, the coherent processing (delay and sum operations) is performed between the modulation (coding) and demodulation (decoding) steps (Figure 1). When dynamic receive focusing delays are used, the synchronization between the modulator and demodulator in the beamformer cannot be maintained. This is a major flaw for the beamformer that significantly reduces the image quality. Different approaches have been proposed to handle this problem, such as multi-bit recoding and modified modulation [29–30], non-uniform oversampling [31], sparse sample processing [36], subfiltering [37], and cascaded filtering [38] based reconstruction.

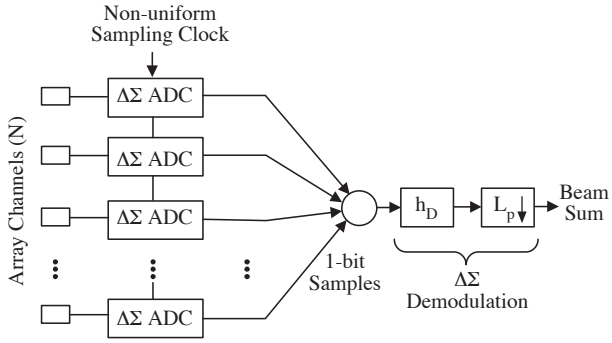

Figure 1. Phased array beamforming using non-uniformly oversampling 1-bit $\Delta\Sigma$ converted data.

Thorough this study, non-uniform oversampling is applied to overcome that problem. In [37] Nilsen and Holm has also presented a theoretical analysis of $\Delta\Sigma$ beamforming from a linear system point of view. Successful FPGA-based realizations of $\Delta\Sigma$ beamforming have been reported recently by Tomov and Jensen [36], Inerfield et al [34], and by Lie and Tanase [35].

2.3. Subarray beamforming

In subarray processing, partial beam sums (low-resolution beams) are acquired from small subarrays, and then these partial beams are coherently processed for producing high-resolution beams (Figure 2). Numerous realizations of subarray beamforming are possible. The basic structure uses a receive subarray multiplexed across a large transducer array with non-overlapping steps, where the transmit subarray is located at the transducer center [24]. A more generalized realization uses partially overlapping multiplexed transmit and receive subarrays [25–26].

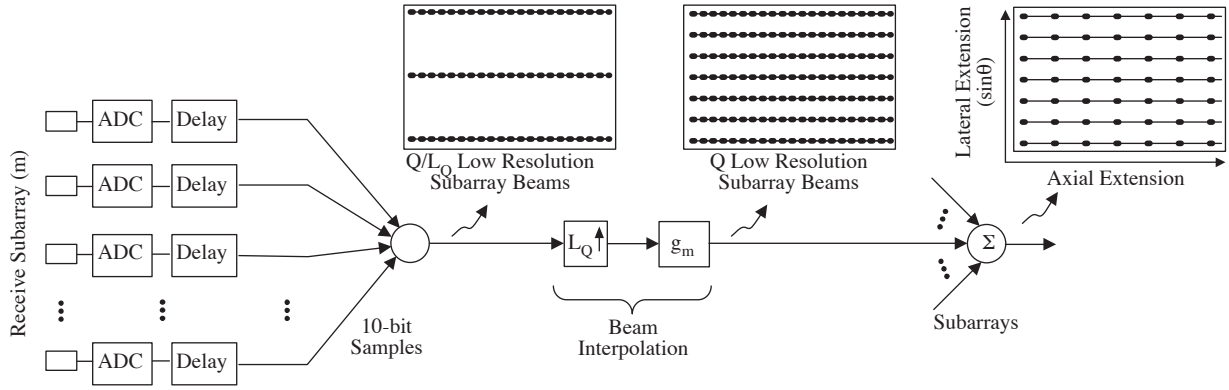

Figure 2. Digital beamforming based on phased subarray processing.

In real-time applications, the number of firings per frame is limited to the acceptable frame rate (Equation 1). In subarray beamforming, the number of firing steps is increased according to the phased array. Therefore, the image space can be sampled coarsely by acquiring a small number of beams proportional to the subarray size, and then the beam density can be increased by beam interpolation prior to coherent summation of subarray beams. The detailed considerations on real-time implementation have been previously discussed [24].

The subarray processing employing N_T (transmit) and N_R (receive) elements subarrays in K successive firings can be expressed by the relation

$$I(p,q) = \sum_{m\ \langle K\rangle} g_m(q) \otimes \sum_{n\ \langle N_R\rangle} \sum_{k\ \langle N_T\rangle} u\left[p - \tau_{n,k}\left(p, \frac{q}{L_Q}\right)\right], \tag{2}$$

where p and q are the indexes representing discretized axial and lateral dimensions (r,$\sin\theta$), respectively; $u(.)$ represents the transmit pulse; $\tau_{n,k}$ includes the receive and transmit beamforming delays; L_Q is the lateral beam upsampling factor; and $g_m(.)$ is a bandpass interpolation filter operating along the lateral dimension (beam index), where the passband is associated with the co-subarray (transmit-receive subarray). In general, for non-overlapping subarrays, the two-way point spread function (PSF) can be approximated by [25] the relation

$$B(\beta) \cong \frac{\sin(2\beta K)}{\sin(2\beta)} \times \frac{\sin(\beta N_T)}{\sin(\beta)} \times \frac{\sin(\beta N_R)}{\sin(\beta)}, \tag{3}$$

where $\beta = (\pi d/\lambda)\sin(\theta)$, d is the inter-element distance, λ is the wavelength, the first term is the response of the synthesized array, and the second and third terms are the responses of the transmit and receive subarrays, respectively. When a fixed transmit subarray at the array center and a multiplexed receive subarray are employed at each firing step, then overall PSF becomes [24]:

$$B(\beta) \cong \frac{\sin(\beta N_T)}{\sin(\beta)} \times \frac{\sin(\beta K N_R)}{\sin(\beta)}, \tag{4}$$

where the first and second terms are the responses of the transmit subarray and the synthesized receive array, respectively. In this case, the PSF of a subarray (with respect to the firing step indice, k) can then be expressed as

$$B_k(\beta) \cong e^{j\Phi_k(\beta)} \frac{\sin(\beta \cdot N_t)}{\sin(\beta)} \frac{\sin(\beta \cdot N_r)}{\sin(\beta)}, \tag{5}$$

where $\Phi_k(\beta)$ is the phase of the k^{th} subarray:

$$\Phi_k(\beta) = \beta\,[2k - K - 1] \cdot N_r. \tag{6}$$

This phase is also the phase of the bandpass beam interpolation filter in lateral direction, mentioned just above.

3. $\Delta\Sigma$ subarray beamforming

A beamforming structure is investigated combining the non-uniform oversampling 1-bit $\Delta\Sigma$ beamforming and the subarray processing structure depicted in Figure 1 and Figure 2, respectively. The $\Delta\Sigma$ subarray beamforming combines both of these methods in a smart way as shown in Figure 3. The processing steps of this structure are as follows: 1) For each subarray, the oversampled, $\Delta\Sigma$ coded partial beam sums are produced by summing the 1-bit data sampled at the time instants corresponding to the focal points; 2) the partial beams are demodulated and decimated using a 1-D low-pass or band-pass filter operating along the axial dimension; 3) the beam density of subarray beams is increased by beam-space interpolation using a 1-D bandpass interpolation filter operating along the lateral dimension; 4) the interpolated beams from all the subarrays are coherently added to produce final high-resolution beams with beam density consistent with the overall synthesized aperture size.

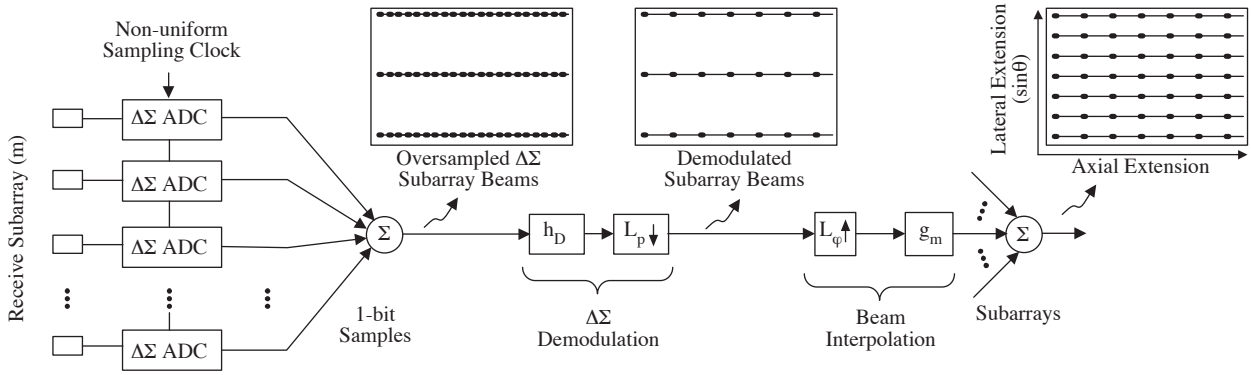

Figure 3. Block diagram of non-uniform oversampling $\Delta\Sigma$ subarray beamforming with the symbolic representation of the beam samples between the processing steps.

The $\Delta\Sigma$ subarray beamforming gets its inputs from subarray structure, therefore the $\Delta\Sigma$ modulated beams are summed and constitute m-bit samples which are still $\Delta\Sigma$ modulated (or coded). $\Delta\Sigma$ demodulation is performed on the m-bit $\Delta\Sigma$ codes. Beam-space interpolation uses multi-bit samples where the high frequency quantization noise is readily removed. Beam space interpolation inserts complex phase into the data, and then the high resolution beams are summed with complex values. The envelope detection can resolve the meaningful information from these complex signals.

The image, $I(.)$, resulting from these processing can be expressed as:

$$I\left(\frac{p}{L_P}, q\right) = \sum_{m\ \langle K\rangle} g_m(q) \otimes \left(h_D(p) \otimes \sum_{n\ \langle N_R\rangle} s_n\left(p, \frac{q}{L_Q}\right)\right), \tag{7}$$

where, L_P is the axial decimation factor; $h_D(.)$ is the demodulation filter (lowpass or bandpass); $s_n(.)$ is the 1-bit $\Delta\Sigma$ coded echo signal at a particular beam angle.

3.1. Comparison of the beamformers

In this subsection, the proposed beamformer is compared with other beamformers according to their hardware complexities. Although the similar results are obtained by each of them, the intermediate steps may differ from one to another.

Different parameters are summarized in the Table 1. First of all, all approaches are compared in their number of active channels. The number of active channels in transmit and receive mode is N for phased array and $\Delta\Sigma$ phased array systems. In subarray and $\Delta\Sigma$ subarray systems this huge number is reduced in transmit mode to N_T, and in receive mode to N_R, where N_T , $N_R << N$. The reduction in channel number is the major significant advantage of the subarray based systems, and hence the proposed one.

On the other hand, the use of data type is also very important for each channel circuitry. In phased array and subarray systems the front-end architecture is 10-bit word length, but in $\Delta\Sigma$ phased array and $\Delta\Sigma$ subarray only 1-bit hardware is needed in each channel. The data types in the internal steps reveal many clues on the approaches. Furthermore, the non-uniformly oversampled $\Delta\Sigma$ beamforming scheme abandons the need for delay circuitry and FIFO buffers for each channel. Thus the front-end hardware becomes simpler.

In phased array and subarray systems, N and N_R delay interpolation filters are used respectively. But in non-uniform $\Delta\Sigma$ beamforming there is no need for delay interpolation filters, because the system is already oversampled. In non-uniform $\Delta\Sigma$ beamforming, only one filter is enough for demodulator step. In overall, non-uniform $\Delta\Sigma$ beamforming is less complex than phased array and subarray systems.

In $\Delta\Sigma$ subarray beamforming, the $\Delta\Sigma$ modulated beams are summed and constitute m-bit samples which are still $\Delta\Sigma$ modulated (or coded). The inputs come from K different non-overlapping subarrays, each has Q/LQ beams. Q/LQ beams are low-pass filtered and decimated. Then, in the beam-space interpolation step, Q/LQ beams are upsampled to Q beams. K low resolution beam images in the *r-sin(θ)* format are summed to final high resolution image.

In subarray systems, the maximum frame rate is decreased in some degree, because the number of firings per frame is increased. But still the final frame rate is acceptable.

3.2. Test results

The image quality of $\Delta\Sigma$ subarray beamforming is tested using an archival RF data set acquired from a test phantom with a 3.5 MHz, 128-element transducer array. The data set consists of all possible RF A-scans from each transmit-receive element combination. A-scan data were sampled at 13.89 MHz with 10-bit resolution. Two different data sets are used. In the first one, the phantom contains six wire targets in water, and is suitable for testing PSFs. The second one is suitable for Contrast to Noise Ratio (CNR) measurements, and has 4 cysts.

2-D B-scan images of the phantoms are reconstructed using 10-bit phased array beamforming, subarray beamforming, phased array with non-uniform oversampling 1-bit $\Delta\Sigma$ beamforming and subarray with non-uniform oversampling 1-bit $\Delta\Sigma$ beamforming. For $\Delta\Sigma$ beamforming, since the oversampling ratio (OSR) critically affects the beamforming Signal to Noise Ratio (SNR), the sampling rate is increased by a factor of 16 to reach an overall OSR=32. In the up-sampling, a low-pass interpolation is performed by inserting zeros into the original sequence and then applying a special low-pass FIR filter with length of 129 (Figure 4). The resulting final sampling frequency becomes 222 MHz.

Table 1. Hardware complexity of different beamformers.

	Phased Array	Non-uniform ΔΣ Phased Array	Subarray	Non-uniform ΔΣ Subarray
# of active channels in transmit mode	N	N	N_T	N_T
# of active channels in receive mode	N	N	N_R	N_R
Type of channel circuitry (front-end)	10-bit	1-bit	10-bit	1-bit
Delay circuitry & FIFO buffer for each channel (front-end)	✓	-	✓	-
Delay interpolation filter	N	-	N_R	-
ΔΣ Demodulation filter	-	1	-	1
# of firings per beam line	1	1	K	K
# of beam lines in acquisition step	Q	Q	Q/L_Q	Q/L_Q
# of beam lines in the result image	Q	Q	Q	Q
Beam interpolation filter	-	-	✓	✓
# of firings per frame	Q	Q	$K \cdot Q/L_Q$	$K \cdot Q/L_Q$
Maximum frame rate	$1/Q \times c/(2 \cdot R)$	$1/Q \times c/(2 \cdot R)$	$L_Q/(K \cdot Q) \times c/(2 \cdot R)$	$L_Q/(K \cdot Q) \times c/(2 \cdot R)$

N: Total receive aperture size; N_R: Number of active receive elements; K: Number of firings (number of receive subarrays); Q: Number of beams; L_Q: Beam upsampling factor.

HARDWARE COMPLEXITY WITH NUMERICAL EXAMPLES

	Phased Array	Non-uniform ΔΣ Phased Array	Subarray	Non-uniform ΔΣ Subarray
# of active channels in transmit mode	96	96	16	16
# of active channels in receive mode	96	96	16	16
Type of channel circuitry (front-end)	10-bit	1-bit	10-bit	1-bit
Delay circuitry & FIFO buffer for each channel (front-end)	✓	-	✓	-
Delay interpolation filter	96	-	16	-
ΔΣ Demodulation filter	-	1	-	1
# of firings per beam line	1	1	6	6
# of beam lines in acquisition step	96	96	32	32
# of beam lines in the result image	96	96	96	96
Beam interpolation filter	-	-	✓	✓
# of firings per frame	96	96	192	192
Maximum frame rate	51	51	25	25

For the illustration of the difference, parameters are taken as follows: N=96; N_R=16; K=6; Q=96; L_Q=3.

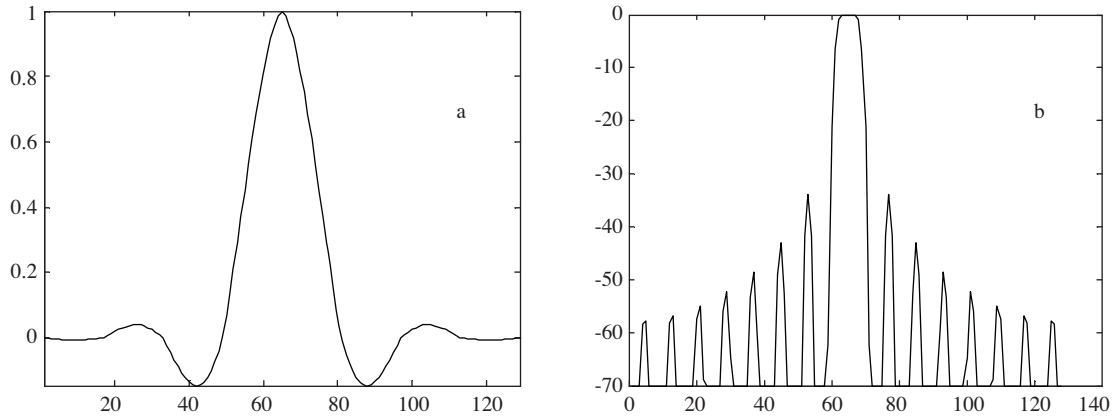

Figure 4. Interpolation filter used in simulating the oversampling effect; a) the coefficients, and b) the frequency response.

The oversampling $\Delta\Sigma$ modulation and digital beamforming was emulated using the interpolated RF data through off-line digital processing. In beamforming, fixed transmit focusing and dynamic receive focusing were employed. The system parameters are listed in Table 2. The parameters of subarray beamforming are taken according to the previous studies [24, 33]. In the subarray processing, the beam interpolation filter length is taken high enough to avoid discontinuities in lateral dimension.

Table 2. System parameters.

Parameter	**Quantity**
Number of active transmit elements (N_T)	16
Number of active receive elements (N_R)	16
Total receive aperture size (N_e)	96
Number of firings per beam line (K)	6
Number of acquired beams (Q/L_Q)	32
Number of interpolated beams (Q)	96
Beam upsampling factor (L_Q)	3
Length of the beam interpolation filter (G_M)	21
Oversampling ratio (L_P)	32
Number of pixels per beam line (P)	512
Length of the demodulation filter (h_D)	281

A second order $\Delta\Sigma$ modulator is used at each receive channel. The $\Delta\Sigma$ demodulation is performed at the output of the partial subarray summation before the beam space interpolation. Firstly, a low-pass filter is applied for the purpose of the demodulation. The coefficients and the frequency response of this filter are shown in Figure 5. It is a 281-tapped filter.

In order to fit the real-time constraints of subarray processing, only a limited number of beam lines are acquired at each firing step. At the final image, more beams than acquired are necessary, and then the other needed beams are obtained by beam space interpolation. For this purpose, a Hamming windowed low pass filter with a complex phase of the corresponding subarray is applied to beams in lateral direction as a band-pass filter ($g_m(.)$). The phase of this bandpass interpolation filter ($\Phi_k(\beta)$) is given in Equation 6. The pass-bands of the beam space interpolation filter is given in Figure 6. After the lateral beam upsampling, the low-resolution images

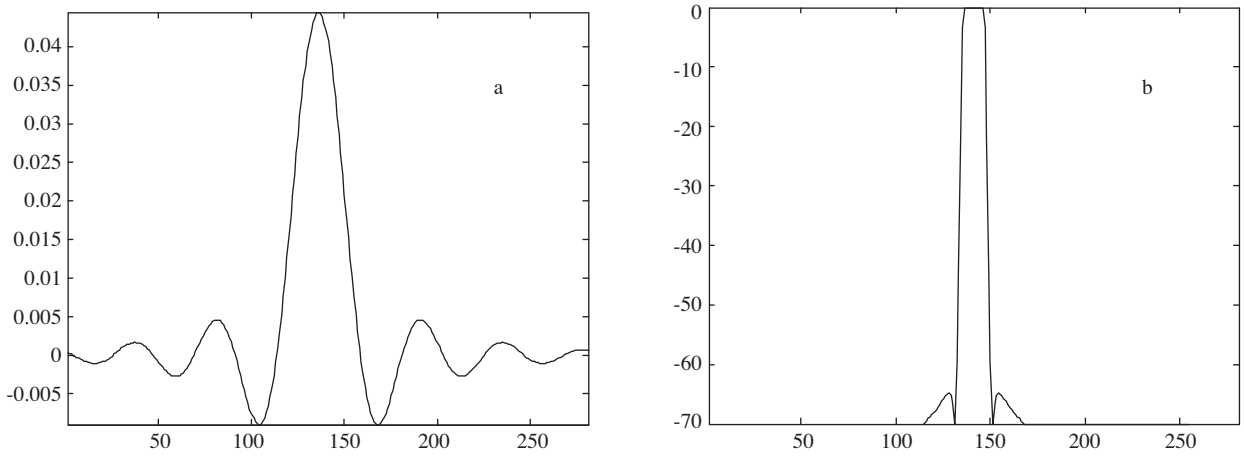

Figure 5. $\Delta\Sigma$ Demodulation filter; a) the coefficients, b) the frequency response.

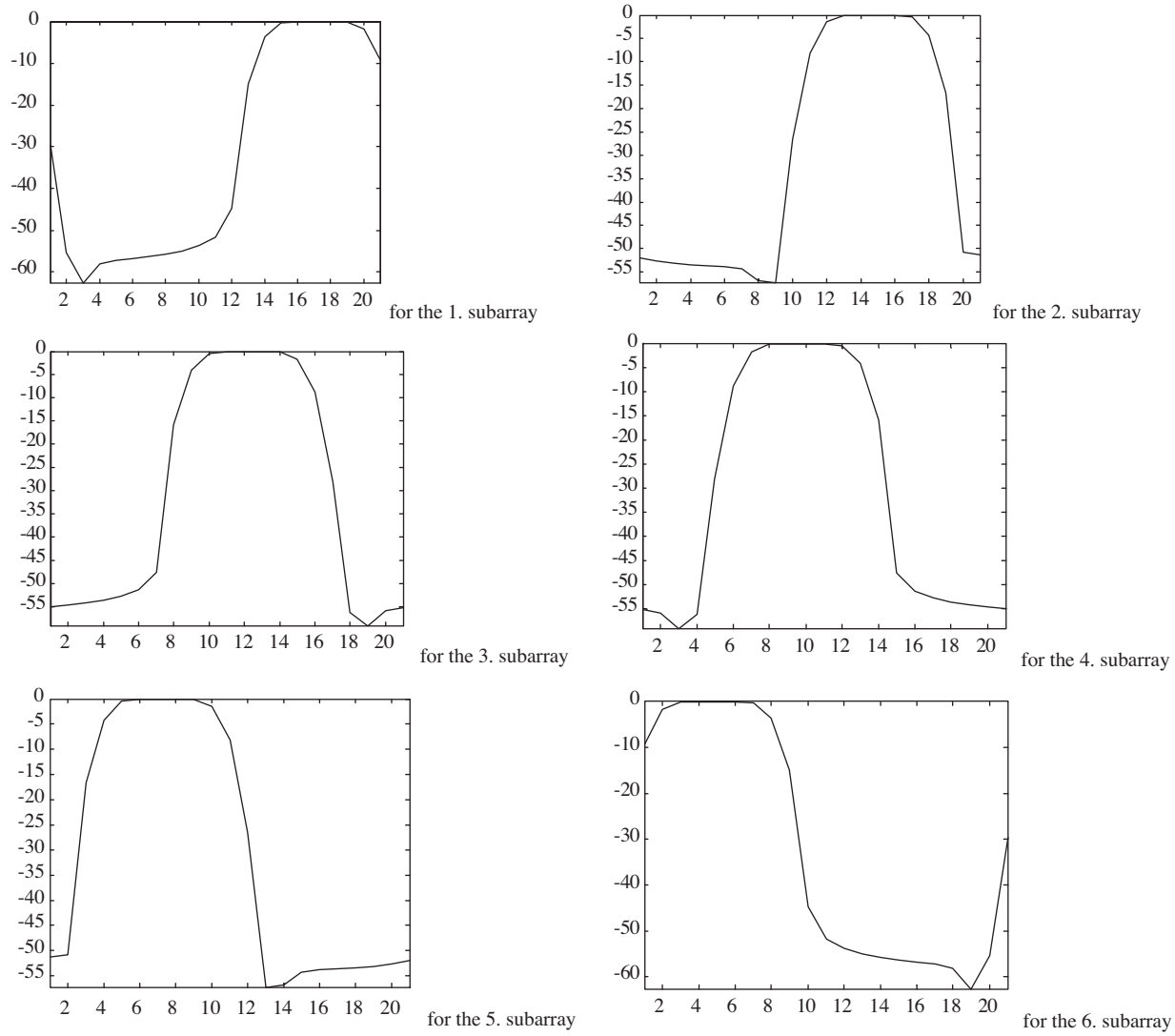

Figure 6. The frequency responses of beam interpolation filters for different subarrays with different pass-band regions.

from subarrays are summed into the high resolution final image. Finally, envelope detection and logarithmic compression were applied to the beamforming outputs.

The reconstructed 2-D B-scan images are presented with 50 dB and 70-dB dynamic ranges in Figure 7.

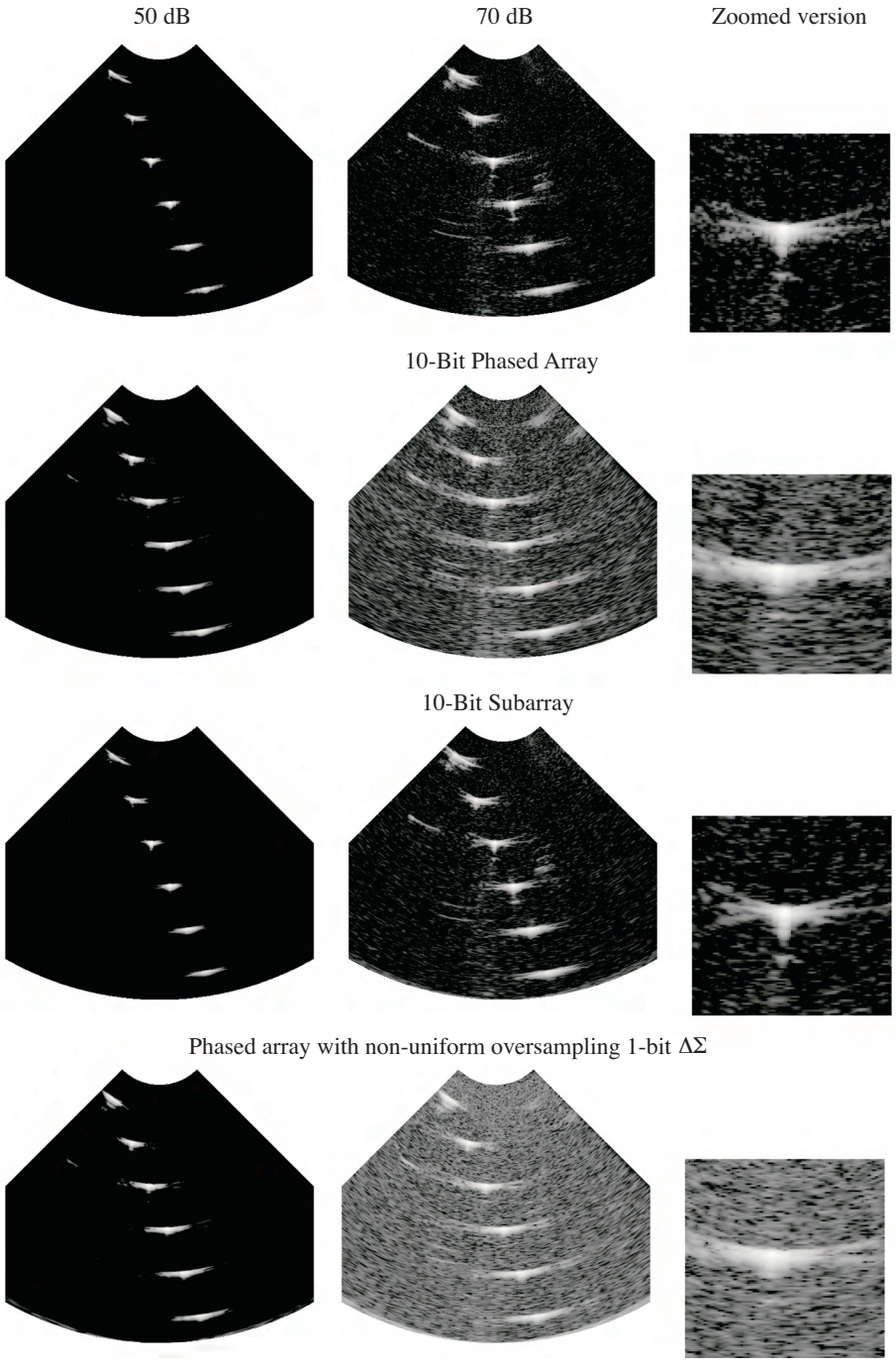

Figure 7. B-scan images of the phantom with six wire targets reconstructed by using different types of beamformers.

In this figure, the phantom with six wire targets is used in order to observe the image quality. The B-scans in the first column are presented with a dynamic range of 50-dB. The subarray image with 50-dB dynamic range depicts the main lobe and near side lobes of PSFs at different depths and scan angles. 10-bit phased array, 10-bit subarray and $\Delta\Sigma$ subarray beamformers produce nearly the same quality image at that range.

To further show the difference between these methods, the same B-scan images at 70 dB are also drawn. At this level, the noise floor becomes more visible in 10-bit subarray and $\Delta\Sigma$ subarray. The zoomed versions of third wires reveal some more details.

To show clearly the relative noise floor levels along the lateral axis, 1-D PSFs are shown in Figure 8. Each 1-D PSF corresponds to the lateral cross-section of 2-D B-scan of the third wire target (from the top). The noise floor of the image reconstructed by the phased array is at about -70 dB. The images reconstructed by the subarray and the $\Delta\Sigma$ subarray have noise floors at -60 dB. The subarray beamforming with non-uniform 1-bit $\Delta\Sigma$ oversampling at the time instants associated with dynamic receive focusing suppresses the quantization noise level below -60 dB.

For quantitative comparison, for each target the image Signal to Noise Ratio (SNR) is calculated as the ratio of the *rms* of pixels in a small window on the main lobe to the of *rms* of pixels in a small window on the side lobe where there is no echo signal. The computed SNRs for the four images are shown in Figure 9. The relative performances of the different beamformers are tested and compared to the gold standard of conventional 10-bit full phased array.

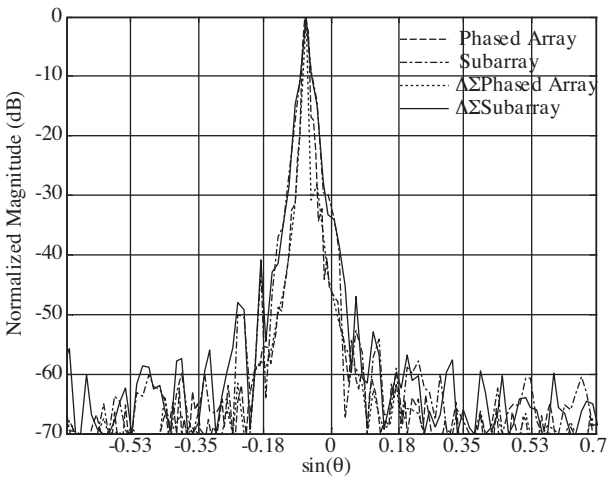

Figure 8. Lateral cross-sections of the B-scan images along the third wire target.

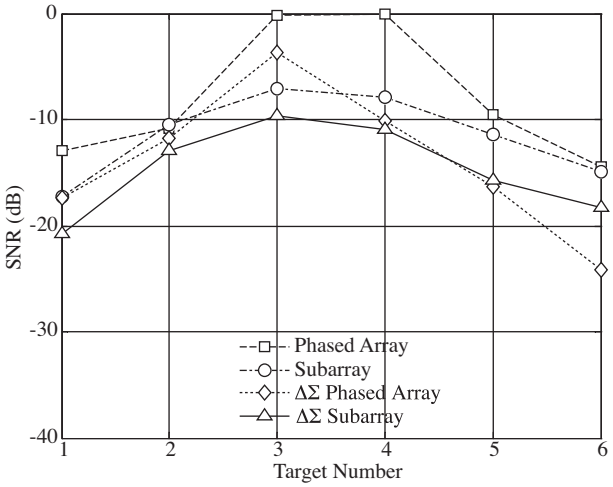

Figure 9. Relative SNR values computed on B-scan images reconstructed by using different types of beamformers.

Figure 9 shows that the SNR performance of the proposed non-uniform oversampling $\Delta\Sigma$ subarray beamformer is about 3 dB poorer than that of the 10 bit subarray beamformer for all the targets. And the overall performance according to the gold standard does not exceed a level of 10 dB difference.

The 1-bit $\Delta\Sigma$ subarray beamformer with uniform oversampling suffers from high quantization noise; the noise floor of its B-scan image is above -40 dB level. These figures are not shown in this study, because such distortion on phased array images has been already investigated in earlier studies [29–31].

In Figure 10, the results that are obtained from cyst phantom are presented. At 50 dB images the

difference between the methods are the most visible. At 70 dB level, all methods give similar image qualities and the difference is undetectable because of the natural noise floor in original data.

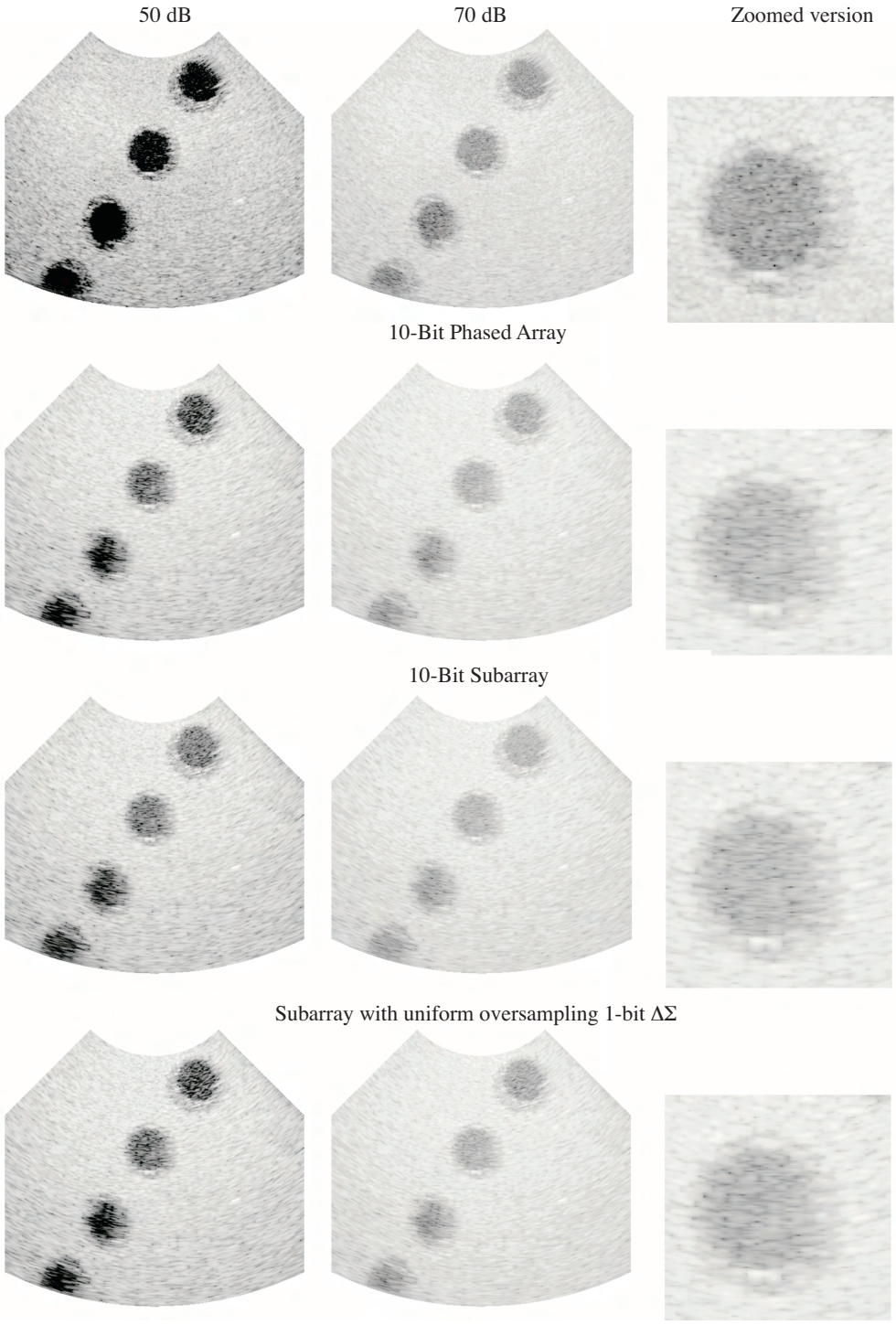

Figure 10. B-scan images of the phantom with 4-cysts reconstructed by using different types of beamformers.

The CNR measurements are very important to show the contrast information. The non-uniform oversampled subarray $\Delta\Sigma$ beamforming has a better performance than the only subarray processing (Figure 11). The CNR values are shown for every 4 cyst separately. In this figure, the CNR values are measured on B-scan images with a dynamic range of 70 dB.

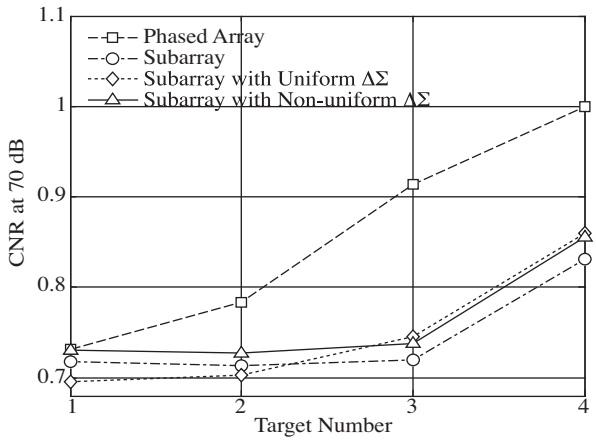

Figure 11. Relative CNR values computed on B-scan images reconstructed by using different types of beamformers.

3.3. Discussion

In $\Delta\Sigma$ subarray beamformer, the $\Delta\Sigma$ demodulation and beam interpolation filters ($h_D(.)$ and $g_m(.)$) are operating along the orthogonal dimensions, r and $\sin\theta$ dimensions, respectively. Therefore altering the sequence of these two operations should not change the beamformer output; it eliminates the demodulation filtering at the subarray outputs, and hence needs demodulation filtering of the overall output only. The processing steps of this modified realization based on this simple principle are as follows: 1) For each subarray, the oversampled, $\Delta\Sigma$ coded partial beam sums are produced by summing the 1-bit data non-uniformly sampled at the time instants corresponding to the focal points; 2) the beam density of subarray beams is increased by beam-space interpolation using a 1-D bandpass interpolation filter operating along the lateral dimension; 3) the subarray beams from all the subarrays are coherently added to produce high-resolution $\Delta\Sigma$ coded beams with beam density consistent with the overall synthesized aperture size; 4) the high-resolution $\Delta\Sigma$ coded beams are demodulated and decimated using a 1-D low-pass or band-pass filter operating along the axial dimension. This is a second approach to combine subarray processing and $\Delta\Sigma$ beamforming which is newly proposed here. The modified realization of $\Delta\Sigma$ subarray can be expressed as

$$I\left(\frac{p}{L_P}, q\right) = h_D(p) \otimes \sum_{m\ \langle K\rangle} \left(g_m(q) \otimes \sum_{n\ \langle N_R\rangle} s_n\left(p, \frac{q}{L_Q}\right)\right) \tag{8}$$

Note that this expression is functionally identical with (7) while the order of the $\Delta\Sigma$ demodulation and beam interpolation are different. The two realizations are expected to produce the identical image quality. In the second approach, beam-space interpolation is performed on K different low resolution images. The number of beams in each low resolution image is increased from Q/L_Q beams to Q beams. After the final summation, $\Delta\Sigma$ demodulation is only once applied to the final high resolution image. In this image, the samples are decimated

to P samples. The second approach has an additional advantage that the beam-space interpolation circuitry can be optimized. In a future study, this part may be implemented without any multiplication. The decision to choose between two realizations of the $\Delta\Sigma$ subarray beamformers is up to the hardware engineers, who may optimize the designs further.

3.4. Conclusion

In this study, a method for non-uniform oversampling 1-bit $\Delta\Sigma$ subarray beamforming was presented. Single-bit oversampling $\Delta\Sigma$ conversion simplifies coherent processing in beamforming with improved timing accuracy. Subarray processing employs small-sized active subarray for beam acquisition, and hence simplifies the beamforming complexity. It requires decimation filtering of partial-beam sums from each subarray. $\Delta\Sigma$ subarray beamforming was tested using archival experimental data. The test results show that the SNR performance of the non-uniform oversampling 1-bit $\Delta\Sigma$ subarray beamformer approaches that of the 10-bit phased array beamformer. Oversampling $\Delta\Sigma$ subarray beamforming can be useful to miniaturize the array front-end and/or to funnel signals to a manageable number of system channels.

References

[1] E. A. Gill, B. Klas, "Three-dimensional echocardiography: an historical perspective," Cardiology Clinics, Vol. 25, No. 2, pp. 221-229, May 2007.

[2] I. S. Salgo, "Three-dimensional echocardiographic technology," Cardiology Clinics, Vol. 25, No. 2, pp. 231-239, May 2007.

[3] O. Oralkan, A. S. Ergun, J. A. Johnson, M. Karaman, B. T. Khuri-Yakub, "Volumetric acoustic imaging using two-dimensional capacitive micromachined transducer arrays," IEEE Trans. Ultrason., Ferroelect., Freq. Contr., vol. 50, no. 11, pp. 1581-1594, Nov. 2003.

[4] B. Savord, R. Solomon, "Fully sampled matrix transducer for real time 3D ultrasonic imaging," IEEE Ultrason. Sympos., pp. 945-953, 2003.

[5] A. F. W. van der Steen, R. A. Baldewsing, F. L. Degertekin, S. Emelianov, M. E. Frijlink, Y. Furukawa, D. Goertz, M. Karaman, P. T. Khuri-Yakub, K. Kim, F. Mastik, T. Moriya, Ö. Oralkan, Y. Saijo, J. A. Schaar, P.W. Serruys, S. Sethuraman, A. Tanaka, H.J. Vos, R. Witte, M. O'Donnell, "IVUS beyond the horizon," EuroIntervention, Issue 5, pp. 132-142, 2006.

[6] J. Schulze-Clewing, M. J. Eberle, D. N. Stephens, "Miniaturized Circular Array," in Ultrasonics Symposium, 2000 IEEE, pp. 1253-1254, 2000.

[7] D. T. Yeh, Ö. Oralkan, I. O. Wygant, M. O'Donnell, B.T. Khuri-Yakub, "3-D Ultrasound imaging using a forward-looking CMUT ring array for intravascular/intracardiac applications," IEEE Trans. Ultrason., Ferroelect., Freq. Contr., vol. 53, no. 6, pp. 1202-1211, June 2006.

[8] F. L. Degertekin, R.O. Guldiken, M. Karaman, "Annular-ring CMUT arrays for forward-looking IVUS: transducer characterization and imaging," IEEE Trans. Ultrason., Ferroelect., Freq. Contr., vol. 53, pp. 474-482, Feb. 2006.

[9] K. E. Thomenius, "Evolution of ultrasound beamformers," in Proc. IEEE Ultrason. Symp., pp. 1615–1622, 1996.

[10] E. Brunner, "How ultrasound system considerations influence front-end component choice," Analog Dialogue, Vol. 36, No. 3, May-July, 2002.

[11] R. Fisher, K. Thomenius, R. Wodnicki, R. Thomas, S. Cogan, C. Hazard, W. Lee, D. Mills B. Khuri-Yakub, A. Ergun, G. Yaralioglu, "Reconfigurable arrays for portable ultrasound," in Ultrasonics Symposium, 2005 IEEE, pp. 495-499, 2005.

[12] R. Fisher, R. Wodnicki, S. Cogan, R. Thomas, D. Mills, C. Woychik, R. Lewandowski, and K. Thomenius, "Packaging and design of reconfigurable arrays for volumetric imaging," Proc. of IEEE Ultrasonics Symposium, pp. 407-410, 2007.

[13] C. R. Hazard, R.A. Fisher, D.M. Mills, L.S. Smith, K.E. Thomenius, and R.G. Wodnicki, "Annular array beamforming for 2-D arrays with reduced system channels," in Ultrasonics Symposium, 2003 IEEE, pp. 1853-1861, 2003.

[14] K. Ranganathan, M. K. Santy, T. N. Blalock, J. A. Hossack, and W. F. Walker, "Direct sampled i/q beamforming for compact and very low-cost ultrasound imaging," IEEE Trans. Ultrason., Ferroelect., Freq. Contr., vol. 51, no. 9, pp. 1082–1094, 2004.

[15] I. Cicek, A. Bozkurt, M. Karaman, "Design of a front-end integrated circuit for 3D acoustic imaging using 2D CMUT arrays," IEEE Trans. Ultrason., Ferroelect., Freq. Contr., vol.52, no. 12, pp. 2235-2241, Dec 2005.

[16] I.O. Wygant, X. Zhuang, D. T. Yeh, O. Oralkan, A. S. Ergun, M. Karaman, and B. T. Khuri-Yakub, "Integration of 2D CMUT arrays with front-end electronics for volumetric ultrasound imaging," IEEE Trans. Ultrason., Ferroelect., Freq. Contr., vol. 55, no. 2, pp. 327-342, Feb. 2008.

[17] G. Gurun, M. S. Qureshi, M. Balantekin, R. Guldiken, J. Zahorian, S.-Y. Peng, A. Basu, M. Karaman, P. Hasler, F. L. Degertekin, "Front-end CMOS electronics for monolithic integration with CMUT arrays: Circuit design and initial experimental results," in IEEE Ultrasonics Symposium, 2008.

[18] M. O'Donnell, M. J. Eberle, D. N. Stephens, J. L. Litzza, K. San Vicente, and B. M. Shapo, "Synthetic phased arrays for intraluminal imaging of coronary arteries," IEEE Trans. Ultrason., Ferroelect., Freq. Contr., vol. 44, pp. 714–721, 1997.

[19] M. Karaman, P. C. Li and M. O'Donnell, "Synthetic aperture imaging for small scale imaging systems," IEEE Trans. Ultrason. Ferroelect. Freq. Contr., vol. 42, no. 3, pp. 429-442, May 1995.

[20] M. Karaman, H. S. Bilge, and M. O'Donnell, "Adaptive multi element synthetic aperture imaging with motion and phase aberration correction," IEEE Trans. Ultrason., Ferroelect., Freq. Contr., vol. 45, pp. 1077–1087, 1998.

[21] K. L. Gammelmark and J. A. Jensen, "Multielement synthetic transmit aperture imaging using temporal encoding," IEEE Trans. Med. Imag., vol. 22, pp. 552–563, 2003.

[22] G. R. Lockwood and F. S. Foster, "Optimising the radiation pattern of sparse periodic two-dimensional arrays," IEEE Trans. Ultrason., Ferroelect., Freq. Contr., vol. 43, pp. 15-19, Jan. 1996.

[23] A. Austeng and S. Holm, "Sparse 2-D arrays for 3-D phased array imaging–design methods," IEEE Trans. Ultrason., Ferroelect., Freq. Contr., vol. 49, pp. 1073–1086, Aug. 2002.

[24] M. Karaman and M. O'Donnell, "Subaperture processing for ultrasound imaging," IEEE Trans. Ultrason. Ferroelect. Freq. Contr., vol. 45, no. 1, pp. 1-10, Jan. 1998.

[25] J. A. Johnson, M. Karaman, B. T. Khuri-Yakub, "Coherent array imaging using phased subarrays—Part I: basic principles," IEEE Trans. Ultrason., Ferroelect., Freq. Contr., vol. 52, no. 1, pp. 37-50, Jan. 2005.

[26] J. A. Johnson, O. Oralkan, A. S. Ergun, U. Demirci, M. Karaman, B. T. Khuri-Yakub, "Coherent array imaging using phased subarrays—Part II: simulation and experimental results," IEEE Trans. Ultrason., Ferroelect., Freq. Contr., vol. 52, no. 1, pp. 51-64, Jan. 2005.

[27] P. M. Aziz, H. V. Sorensen, and J. V. Spiegel, "An overview of delta-sigma converters," IEEE Signal Proces. Mag., vol. 13, no. 1, pp. 61-84, Jan. 1996.

[28] O. Norman, "A band-pass delta-sigma modulator for ultrasonic imaging at 160 MHz clock rate," IEEE J. Solid-State Circuits, vol. 31, no. 12, pp. 2036–2041, 1996.

[29] S. R. Freeman, M.K. Quick, M. A. Morin, R. C. Anderson, C. S. Desilets, T. E. Linnenbrink, and M. O'Donnell, "Delta-sigma oversampled ultrasound beamformer with dynamic delays," IEEE Trans. Ultrason., Ferroelect., Freq. Contr., vol. 46, no. 2, pp. 320-332, Mar. 1999.

[30] S. R. Freeman, M. K. Quick, M. A. Morin, R. C. Anderson, C. S. Desilets, T. E. Linnenbrink, and M. O'Donnell, "Heterodyning technique to improve performance of delta-sigma-based beamformers," IEEE Trans. Ultrason., Ferroelect., Freq. Contr., vol. 46, no. 4, pp. 771–790, 1999.

[31] M. Kozak, and M. Karaman, "Digital phased array beamforming using single-bit delta-sigma conversion with non-uniform oversampling," IEEE Trans. Ultrason., Ferroelect., Freq. Contr., vol. 48, no.4, pp. 922-931, July 2001.

[32] H.S. Han, H.J. Park, T.K. Song, "A new architecture for ultrasound sigma-delta modulation beamformer," Proceedings IEEE Ultrasonics Symposium, vol.2, pp.1631-1634, Oct. 2002.

[33] H.S. Bilge, and M. Karaman, "Subarray delta-sigma beamforming for ultrasonic imaging," Proceedings of the IEEE Ultrasonics Symposium, vol.2, pp. 1623-1626, Oct. 2002.

[34] M. Inerfield, G. R. Lockwood, S. L. Garverick, "A sigma-delta-based sparse synthetic aperture beamformer for real-time 3-D ultrasound," IEEE Trans. Ultrason., Ferroelect., Freq. Contr., vol. 49, no. 2, pp. 243-254, Jan. 2002.

[35] I. Lie, M.E. Tanase, "About the possibility to implement a nonuniform oversampling receive beamformer in a FPGA," Proceedings of the IEEE Ultrasonics Symposium, vol. 2, pp. 1404-1407, Sept. 2005.

[36] B.G. Tomov, J.A. Jensen, "Compact FPGA-based beamformer using oversampled 1-bit A/D converters," IEEE Transactions on Ultrasonics, Ferroelectrics and Frequency Control, vol. 52, issue 5, pp. 870-880, 2005.

[37] C.I.C. Nilsen, S. Holm, "Distortion-free delta-sigma beamforming," IEEE Trans. Ultrason., Ferroelect., Freq. Contr., vol. 55, no. 8, pp. 1719-1728, Aug. 2008.

[38] J.H. Cheong, Y.Y.H. Lam, K.T. Tiew, L.M. Koh, "Sigma-delta receive beamformer based on cascaded reconstruction for ultrasound imaging application," IEEE Trans. Ultrason., Ferroelect., Freq. Contr., vol. 55, no. 9, pp. 1935-1946, Sep. 2008.